JCIM JOURNAL OF CHEMICAL INFORMATION AND MODELING

Article

pubs.acs.org/jcim

Fatty Acid and Retinol-Binding Protein: Unusual Protein Conformational and Cavity Changes Dictated by Ligand Fluctuations

G. P. Barletta,[†] G. Franchini,[‡] B. Corsico,[‡] and S. Fernandez-Alberti*[,†]

[†]Universidad Nacional de Quilmes/CONICET, Roque Saenz Peña 352, B1876BXD Bernal, Argentina

[‡]Instituto de Investigaciones Bioquímicas de La Plata, CONICET-UNLP, Facultad de Ciencias Médicas, calles 60 y 120 s/n, 1900 La Plata, Argentina

S *Supporting Information*

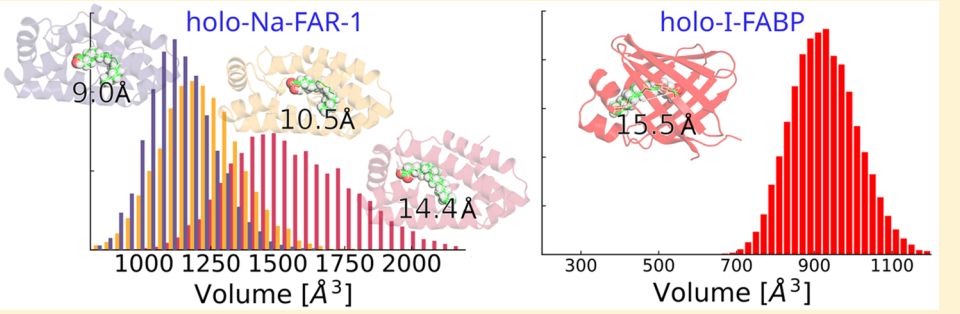

ABSTRACT: Lipid-binding proteins (LBPs) are soluble proteins responsible for the uptake, transport, and storage of a large variety of hydrophobic lipophilic molecules including fatty acids, steroids, and other lipids in the cellular environment. Among the LBPs, fatty acid binding proteins (FABPs) present preferential binding affinities for long-chain fatty acids. While most of FABPs in vertebrates and invertebrates present similar β-barrel structures with ligands accommodated in their central cavity, parasitic nematode worms exhibit additional unusual α-helix rich fatty acid- and retinol-binding proteins (FAR). Herein, we report the comparison of extended molecular dynamics (MD) simulations performed on the ligand-free and palmitic acid-bond states of the *Necator americanus* FAR-1 (Na-FAR-1) with respect to other classical β-barrel FABPs. Principal component analysis (PCA) has been used to identify the different conformations adopted by each system during MD simulations. The α-helix fold encompasses a complex internal ligand-binding cavity with a remarkable conformational plasticity that allows reversible switching between distinct states in the holo-Na-FAR-1. The cavity can change up to one-third of its size affected by conformational changes of the protein−ligand complex. Besides, the ligand inside the cavity is not fixed but experiences large conformational changes between bent and stretched conformations. These changes in the ligand conformation follow changes in the cavity size dictated by the transient protein conformation. On the contrary, protein−ligand complex in β-barrel FABPs fluctuates around a unique conformation. The significantly more flexible holo-Na-FAR-1 ligand-cavity explains its larger ligand multiplicity respect to β-barrel FABPs.

1. INTRODUCTION

Hydrophobic lipophilic molecules like fatty acids, steroids, retinoids, and their derivatives participate in a large variety of functions within a cell, including energy storage, signaling, regulation of gene expression, hormonal roles, and membrane permeability regulation among others. Their insolubility in water and their potential oxidative degradation require their coordinated transport and availability, protection and regulation throughout the hydrophilic intracellular environment. Soluble lipid-binding proteins (LBPs) are a group of abundant proteins that are responsible for these tasks throughout the aqueous environment inside numerous types of cells[1] and body fluids of different organisms.[2] Helminth parasites have a restricted lipid metabolism and must acquire simple and complex lipids from their hosts,[3] therefore LBPs probably perform very important functions for parasite growth and development.

Fatty acid and retinol binding proteins (FARs) are LBPs that have been described as components of E/S fluids from parasitic nematodes[4−7] and they are hypothesized to play essential roles in lipid acquisition and distribution of nutrients as well as potential dampening of host's immune response.[8,9] FARs together with nematode polyprotein/allergens (NPAs)[10] are small (14−20 kDa), helix rich proteins that bind retinol and fatty acids and have no recognizable counterparts in other animal groups.[2] Given these characteristics, FARs have been proven to be useful for serodiagnosis and experimental

Received: April 29, 2019
Published: July 31, 2019

 © XXXX American Chemical Society

DOI: 10.1021/acs.jcim.9b00364
J. Chem. Inf. Model. XXXX, XXX, XXX−XXX

vaccines.[11−13] Moreover, there is evidence that FARs from filarial nematodes are able to bind anthelmintic drugs.[14,15]

Hookworm disease is a highly debilitating helminth infection that is related to iron deficiency anemia (IDA) in tropical developing countries with an estimated prevalence of 451 million cases that cause 1.6 million years lived with disability (YLD).[16] *Necator americanus*, together with *Ancylostoma duodenale* and *Ancylostoma ceylanicum*, are the causative agents for the above mention "hookworm disease". It is important to note that *N. americanus* is responsible for the majority of cases worldwide. This parasitosis has been successfully eradicated from developed countries by mass drug treatments and by economic development.[17] Nevertheless the levels of disease burden remains high in many low middle income countries like the north region of Argentina.[18]

FARs occur in several isoforms, and Na-FAR-1 has been found to be highly expressed in the adult form.[19,20] At the present time, two orthologues FAR structures were solved, one from *Necator americanus* (Na-FAR-1 by protein nuclear magnetic resonance (NMR) and X-ray crystallography; PDB: 4UET and 4XCP, respectively)[20] and another from *Caenorhabditis elegans* (Ce-FAR-7, by X-ray crystallography; PDB: 2W9Y).[21] Both present similar overall α helix-rich structures with certain structural differences. Particularly, the size and shape of their internal cavities are different, denoting differences in their ligand selectivity. Na-FAR-1, in either its apo- and holo-conformations, presents a larger and more complex internal ligand-binding cavity.[20]

Among soluble LBPs, another interesting group is the fatty acid binding proteins (FABPs) family presenting preferential binding affinities for long-chain fatty acids.[22−27] While FARs have been found exclusively in nematodes[28] FABPs can be found in vertebrates and invertebrates. Despite their low sequence identity and their functional divergence, probably related to their particular lipid-binding preferences, they share a common tertiary structure.[29,30] They all have similar β-barrel structures that encase the bound fatty acid. The volume of the inner ligand-binding cavity is determined by the side chains of the residues that define the molecular surface enclosing it. These residues vary between the different FABP types, and they determine the ligand specificity of the cavity. Various single point mutations, performed on residues lining the cavity of different FABP types, have shown to modify the protein conformational stability, ligand specificity and affinity.[31−36] Several studies, based on crystal and solution analysis, predicted the way FAs enter and leave the FABP binding site;[24,37] this is fundamental to understanding the molecular mechanism of ligand selection and delivery in FABPs.[38,26,39−42] These works have shown the importance of certain residues and domains in the protein dynamics, confirming observations performed by different experimental methods and allow to hypothesize about these protein's proposed functions in the cell. While nematodes also produce β-barrel FABPs, the reasons why nematodes have specialized in the use of α-helix rich proteins remain unclear.

An understanding of how the conformational diversity of FARs contributes to their ligand multiplicity, varying the relative affinities for different hydrophobic lipophilic molecules, could enlighten their roles in parasitism and suggest possible targets for therapeutic interventions. Fluorescence-based ligand-binding assays and titration of Na-FAR-1 with sodium oleate monitored by NMR reveal its high ligand multiplicity.[20] These studies suggest the higher propensity of the α-helical fold to bind a larger variety and quantity of FAs and other lipid classes than the β-barrel fold. Besides, Na-FAR-1 ligand-binding induces substantial chemical shift changes for residues throughout the protein, indicating significant conformational changes that allow the structure to expand.

Molecular dynamics (MD) simulations[43−46] combined with principal component analysis (PCA)[47−51] provide a framework for decomposing the complexity of proteins motions into decoupled individual contributions. PCA is a useful multivariate statistical method that has been applied to reduce the number of dimensions needed to describe protein dynamics. This combination of MD and PCA has recently been applied to develop a procedure that reveals the existence of correlations between the dynamics of cavities and structures.[52,53] Besides, MD simulations have shown to be the adequate computation method to reveal several dynamic and functional aspects of LBPs,[54,55,40,56] like ligand entry and leave pathways and complex formation,[26,39,57] and binding-relevant intermediate states.[42] Moreover, MD simulation of the flexibility of the internal cavity has shown to be a requirement for a good simulation of ligand-LBPs affinities.[58]

Herein we explore the structure-dynamics-function relationship of Na-FAR-1 using long molecular dynamics simulations combined with PCA in its *apo*- and *holo*-forms. We analyze its plasticity and the impact of the different conformations on the ligand-binding cavity volume. We were focused on the dynamics relationships between protein fluctuations, cavity changes, and the enclosed ligand different conformations. A comparison of our results with those obtained from MD simulations of the rat intestinal fatty-acid-binding protein (I-FABP) with the typical FABP β-barrel fold, and the orthologue Ce-FAR-7 is performed. Our analysis reveals that Na-FAR-1 encompasses a complex internal ligand-binding cavity with a remarkable conformational plasticity that allows reversible switching between distinct states according with the enclosed ligand different conformations.

2. METHODS

2.1. Molecular Dynamics simulations. Molecular dynamics (MD) simulations were performed for Na-FAR-1 and I-FABP, both in their *apo*- and *holo*- forms with palmitate in their binding pockets, and Ce-FAR-7 in its unligated form. These were carried out with AMBER 16 software package,.[59,60] Initial structures for each protein were obtained from the protein data bank[61] (pdb id 4UET (no. of atoms = 23173) and 4XCP (no. of atoms= 22707) for *apo*- and *holo*-Na-FAR-1[20] respectively, 1IFB[62] (no. of atoms = 15502) for *apo*-I-FABP, 2IFB[63] (np. of atoms = 15768) and 1URE[64] (no. of atoms = 16143) for *holo*-I-FABPs and 2W9Y[21] (no. of atoms 21528) for *apo*- Ce-FAR-7). Each protein was solvated with explicit water molecules in a rectangular periodic box large enough to contain the protein and 10 Å of solvent on all sides. Ions are added for charge neutralization. Periodic boundary conditions and particle-mesh Ewald (PME) sums were applied. The AMBER ff14SB[65,66] force field and the TIP3P[67] water model were used in all simulations. Minimization of each system was performed in two steps: first, constraints were applied to the protein atoms and 200-steps of steepest-descent and 800-steps of conjugate gradient minimization were run; then, constraints are lifted and the same procedure were applied again. This was followed by 400 ps of heating to reach the final temperature of 300 K. During heating a harmonic constraint of 25.0 (kcal/mol)/Å^2 was applied to the protein atoms. The time step was 2

DOI: 10.1021/acs.jcim.9b00364
J. Chem. Inf. Model. XXXX, XXX, XXX−XXX

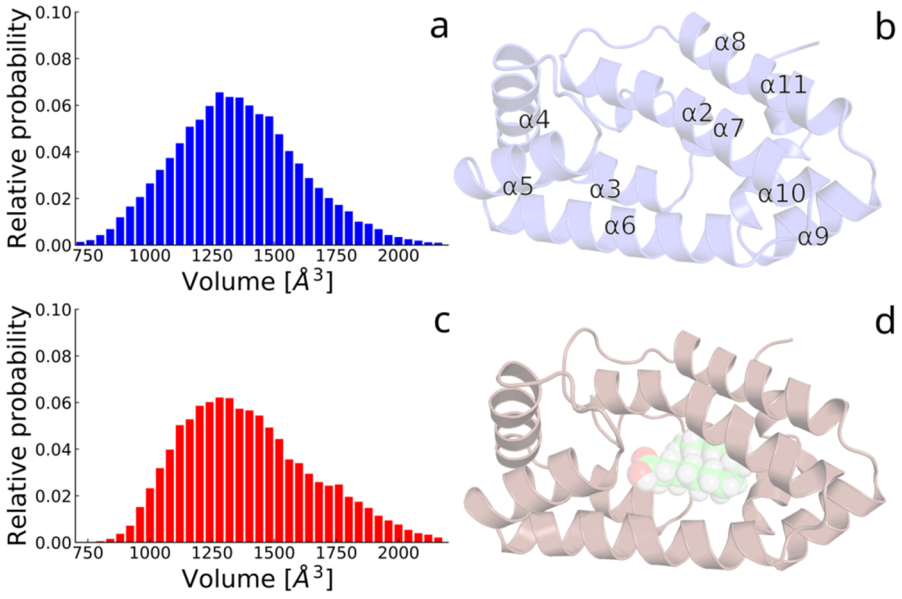

Figure 1. Averaged (b) *apo*- and (d) *holo*-structures for Na-FAR-1 obtained from the corresponding equilibrated MD simulations, indicating the main secondary structure elements (SSE) and the encompassed ligand cavity. Distribution of ligand cavity volumes, calculated over the set of structures collected during the equilibrated MD simulations of (a) *apo*- and (c) *holo*-Na-FAR-1.

fs, and the SHAKE algorithm was employed to constrain bonds involving hydrogen atoms. A cutoff of 10 Å was applied to nonbonded interactions. Systems were equilibrated for 7.8 ns at constant pressure gradually reducing the constraints every 100 ps until all restraints were lifted. After that, the systems were equilibrated at the constant temperature of 300 K using the Andersen barostat and the Langevin thermostat with a γ collision frequency of 2 ps^{-1} during 12.2 ns. Finally, 3-μs production MD runs were performed, during which configurations were collected at 10 ps intervals.

2.2. Principal Component Analysis. PCA is an extensively used statistical procedure to identify the essential dynamics from MD simulations[47−51,68] and, thereby, facilitate the study of long time dynamics. For the sake of consistency, we briefly review PCA below.

Herein, PCA modes $\mathbf{Q}_i$ are $3N$ orthogonal eigenvectors obtained as columns of the eigenvector matrix $\mathbf{L}$, that results after diagonalizing ($\mathbf{L}^T\mathbf{C}\mathbf{L} = \mathbf{\Lambda}$) the covariance matrix of atomic fluctuations $\mathbf{C}$ whose elements are defined as

$$C_{ij} = \langle q_i q_j \rangle = \frac{1}{K}\sum_{k=1}^{K} q_i^k q_j^k \quad (1)$$

where the sum goes over the K configurations stored during previously equilibrated MD simulations, $q_i^k = \sqrt{m_i}(x_i^k - \langle x_i \rangle)$ is the mass-weighted internal displacement of Cartesian coordinate x_i^k of the ith atom (i = 1, ..., N; N = number of residues in the protein (C_α) with mass m_i, and the angular brackets represent the average obtained from the K configurations.[68] The elements of the diagonal matrix $\mathbf{\Lambda}$ represent the relative contribution of each PCA or essential mode (EM) to the overall fluctuation of the molecule. The eigenvectors are typically ordered according to descending eigenvalues, with the first PCA mode being the one with major contribution.

2.3. Ligand-Cavities: Definition, Volume, and Flexibility. Ligand-cavities have been defined by visual inspection of the average of equilibrated MD structures and previous knowledge on each system. The complete list of residues lining the main ligand-binding cavity for each system is provided in the Supporting Information (Table S1).

Cavity volumes are calculated using our previously developed method,[53] particularly suited to measure changes in cavity volumes due to small atomic coordinate displacements in the direction of specific predefined directions of protein structural displacements. Following our previous works we make use of the volume gradient vector ($\nabla\mathbf{V}_{ol}$), defined as the vector of partial derivatives of the cavity volume in the basis of PCA modes $\{\mathbf{Q}_i\}_{i=1,3N}$, that is

$$\nabla\mathbf{V}_{ol} = \sum_{i=1}^{3N} c_i\mathbf{Q}_i = \sum_{i=1}^{3N}\frac{\partial V_{ol}}{\partial Q_i}\mathbf{Q}_i \quad (2)$$

Within the frame of the quasi-harmonic analysis approximation,[69] the variation of the potential energy of a protein in the direction of $\nabla\mathbf{V}_o$ is defined as

$$\nabla E_{\nabla\mathbf{V}_{ol}} = \sum_{i=1}^{3N}\Delta E_{\mathbf{Q}_i} \quad (3)$$

with

$$\Delta E_{\mathbf{Q}_i} = \frac{1}{2}k_i c_i^2 \Delta X^2 \quad (4)$$

being $k_i = \frac{k_B T}{\lambda_i}$, k_B the Boltzmann constant and T the absolute temperature (300 K). ΔX represents a relative displacement in the direction of $\nabla\mathbf{V}_{ol}$. Therefore, we consider $\Delta E_{\nabla\mathbf{V}_{ol}}$ as measure of flexibility of the cavities.

3. RESULTS AND DISCUSSION

3.1. α-Helix Rich FARs. While most of FABPs present a β-barrel folding, FARs reveals an unusual α-helical fold. In the case of Na-FAR-1, it consists of a wedge-shaped structure composed of 11 helices with different lengths that enclose an internal ligand-binding cavity. The overall ligand-binding conformational change involve a global RMSD of 0.98 Å

DOI: 10.1021/acs.jcim.9b00364
J. Chem. Inf. Model. XXXX, XXX, XXX−XXX

between conformers, calculated from the α-carbons superposition of averaged *apo*- and *holo*-structures obtained from the corresponding equilibrated MD simulations (see Figure 1b,d). Both *holo*-states for Na-FAR-1 and I-FABP are bound to a single molecule of palmitate. It is important to note that this is the preferred ligand of Na-FAR-1 in a biological environment[20] The main structural distortions upon ligand binding are localized on helices 3_{10}, α2, α7, α10 and the loops between 3_{10}-α2, α2-α3, α4-α5, and α7-α8. Among these Secondary Structure Elements (SSE), α4-α5 and α7-α8 have shown the largest root-mean-square fluctuations (RMSF; see Figure S1) during our MD simulations, particularly residues 39−45 in α4-α5 loop and residues 100−103 in α7-α8 loop present the largest relative flexibility. The structural change of α4-α5 loop during ligand-binding is expected since this loop is part of the single opening of the ligand-binding cavity, located between this loop and helices α6 and α7. Besides this opening, α7-α8 loop has been previously proposed[20] as the main candidate to participate of the ligand entrance through the portion of the cavity accessible to solvent.

At this point it is interesting to note that the RMSD between average holo- and apo- structures of Na-FAR-1 is only 1.58 Å. Nevertheless, in a previous article,[70] we have pointed out that small structural distortions can involve large changes in the cavities of the proteins. Besides, in cases that proteins explore multiple conformers during MD simulations, the average structural is not a good statistics. Therefore, in what follows, the identification of different conformers and their impact on the ligand-cavity is discussed.

A further inspection of the internal ligand-binding cavity can be seen in Figure 1a,c where the distributions of cavity volumes, calculated over the set of structures collected during the equilibrated MD simulations of *apo*- and *holo*-Na-FAR-1, are shown. Their average values are 1353 ± 254 and 1397 ± 266 Å^3 respectively. These values differ from the corresponding 940 and 2170 Å^3 calculated on the initial experimental structures.[20] As we have pointed out previously, we define internal cavities according to average structures obtained from our MD simulations. The distributions shown in Figure 1a,c are the result of the protein thermal fluctuations that can involve different conformational changes throughout the 3-μs of MD simulations. Fluctuations of helices that form the cavity introduce relatively small protein structural rearrangements that can lead to significant changes on the internal cavity size.[70] Histograms shown in Figure 1a,c reveal that internal cavity can duplicate its volume due to protein fluctuations. While the distribution of volume cavities for *apo*-Na-FAR-1 corresponds to a Gaussian distribution that can be associated with thermal fluctuations around a unique protein conformation, this is not the case for *holo*-Na-FAR-1.

Volume cavity changes can be associated with protein fluctuations. Therefore, in order to elucidate this feature, MD simulations were analyzed in terms of PCA. The first and second PCA modes of *apo*- and *holo*-Na-FAR-1are shown in Figure 2a,b. In both conformers, the first 2 modes involve the concerted motion of residues located in helices α4, α5, the loop between, and the C-term of the helix α7. In agreement with previous experimental observations,[20] the last helix has the most impact on cavity volume, while the former form the ligand entrance gate (α4-α5 gate).

Figure 3a,b show the projection of the set of MD snapshots of *apo*- and *holo*-Na-FAR-1 onto their corresponding first and second PCA modes. Thermal fluctuations of *apo*-Na-FAR-1 are

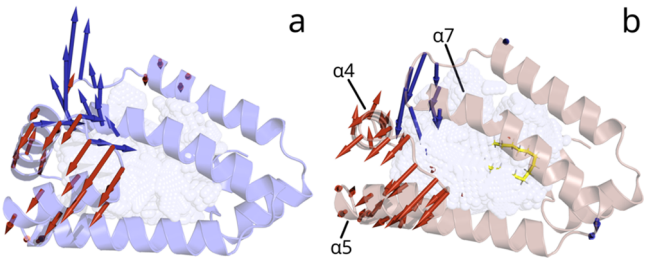

Figure 2. 1st (red) and 2nd (blue) PCA modes of (a) *apo*- and (b) *holo*-Na-FAR-1.

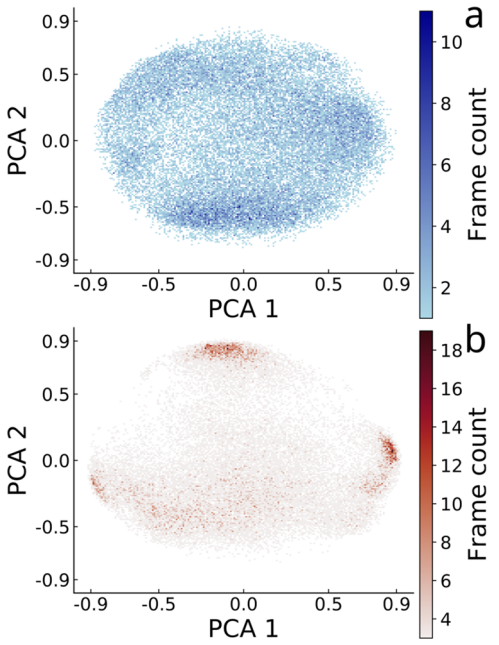

Figure 3. Contour density plots of the projection of the set of MD snapshots of (a) *apo*- and (b) *holo*-Na-FAR-1 onto their corresponding 1st and 2nd PCA modes.

revealed as gradual combinations of both modes without showing significant prevalence of structural distortions in any specific direction. That is, *apo*-Na-FAR-1 does not visit any new conformation that persists a significant amount of time during the MD simulation. On the contrary, we can observe that *holo*-Na-FAR-1 actually evidence the existence of three different conformers: two stable conformers presenting structural distortions mainly in both senses of the direction of the first PCA mode (conformers A and B), and a third conformer C in the direction of the second PCA mode. The projections of the set of MD snapshots of apo- and holo-Na-FAR-1 onto their corresponding third PCA modes do not show the existence of new stable conformers with structural distortions in the direction of these modes (see Figure S2). The major differences among conformers A, B, and C lie in the α4-α5 gate and the helix α7. Conformer A's α7 helix is relatively straightened, allowing the α4-α5 gate to close up. B's α7 helix has a kink next to its C-term around ILE 104, which displaces the α4-α5 gate. This kink is even steeper in Conformer C. This kink is the main reason for the volume decrease in conformers B and C (see Figure 4a). Therefore, the distribution of internal cavity volumes shown in Figure 1c can be interpreted as the contribution of three different conformations explored by *holo*-Na-FAR-1 during the MD

DOI: 10.1021/acs.jcim.9b00364
J. Chem. Inf. Model. XXXX, XXX, XXX−XXX

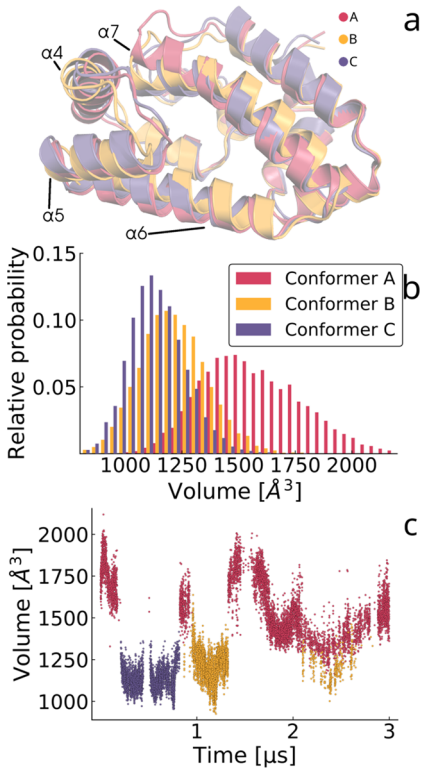

Figure 4. (a) Superposition of the three conformers (A, B, and C) of holo-Na-FAR-1; (b) distribution of cavity volumes for each of the conformers (A, B, and C) of *holo*-Na-FAR-1 during the MD simulation; (c) evolution in time of the cavity volume displaying the different contributions of each of the three A, B, and C conformers.

simulation. Figure 4b shows the distribution of cavity volumes for each of them. While two of the *holo*-Na-FAR-1conformers (B and C) enclose relative small internal cavities with average volumes of 1130 ± 126 and 1211 ± 150 Å^3, the other conformer (A) presents a large cavity of 1568 ± 222 Å^3. These results indicate that *holo*-Na-FAR-1 presents a remarkable conformational plasticity that drives a complex internal cavity dynamics. The three identified conformers are in dynamical equilibrium connected by conformational changes involving the first and the second PCA modes. Figure 4c shows the evolution in time of the cavity volume displaying the different contributions of each of the three conformers. Reversible interconversions between them can be observed during the MD simulation. These results are in complete agreement with our previous analysis of the *apo* and *holo* structures of Na-FAR-1 employing NMR spectroscopy.[20] In the referred work, NMR spectra of *holo*-Na-FAR-1 in solution, like those of other FAR proteins previously tested, were characterized by broad signal peaks indicative of multiple conformations and/or conformational exchange. However, *apo*-Na-FAR-1gave good solution NMR spectra which allowed the structure of apo-Na-FAR-1 to be determined. In the same work the ligand binding process was followed through NMR and showed that the protein exhibited slow exchange behavior through the addition of 1, 2, and 3 mol equiv of the ligand (oleate), which would suggest that the protein binds three ligands with high affinity. The higher plasticity of the protein after the incorporation of one molecule of ligand, as shown in the present work, would eventually make the protein more susceptible to accept more ligand molecules.

In order to further understand the effect of higher conformational plasticity of *holo*-Na-FAR-1 respect to *apo*-Na-FAR-1 on the ligand binding, the dynamics of the ligand within the cavity has been explored. For this purpose, ligand structural fluctuations have been analyzed using PCA. Figure 5(a) shows the projection of the ligand structures, obtained

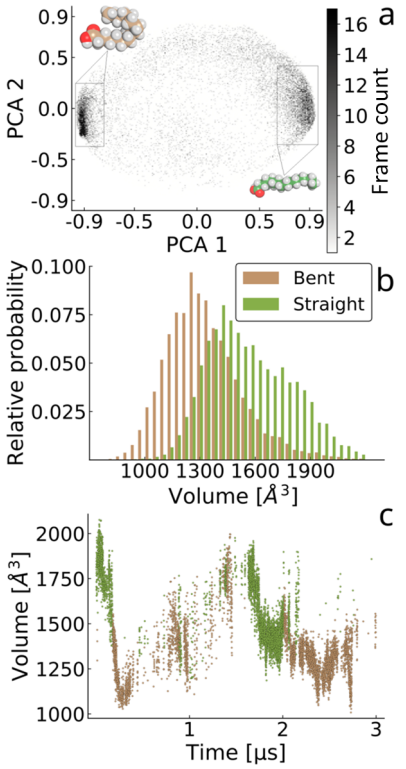

Figure 5. (a) Contour density plots of the projection of the palmitate structures, obtained from the set of MD snapshots of *holo*-Na-FAR-1, onto its 1st and 2nd PCA modes; (b) distribution of cavity volumes according to the conformation of the ligand encompassed in it; (c) evolution in time of the cavity volume displaying the different conformations adopted by the ligand.

throughout the MD simulation, onto its first and second PCA modes. Two distinctive ligand conformations represented by the structural distortions in both senses of the direction of the first PCA mode can be observed. They correspond to the bent and stretched conformations shown in Figure 5a. As can be seen in Figure 5b, the ligand fluctuates between them, being the stretched conformation associated with large cavity volumes while the bent one is observed within smaller cavity volumes (Figure 5c). That is, far from being fixed within the cavity, the ligand experiences large conformational changes associated with changes of cavity volume.

The relationship between the different *holo*-Na-FAR-1 conformers, with their corresponding associated changes in the internal cavity volume, and the different ligand conformations can be analyzed by depicting the distribution of distances between the extremes of the palmitate molecule, that is, the distance from the C atom of carboxyl group to the C atom of the methyl group (see Figure 6). We can observe that the stretched palmitate conformation is associated with the *holo*-Na-FAR-1 conformer (A) with the largest internal cavity and the straightened α7 helix to make room for the

DOI: 10.1021/acs.jcim.9b00364
J. Chem. Inf. Model. XXXX, XXX, XXX−XXX

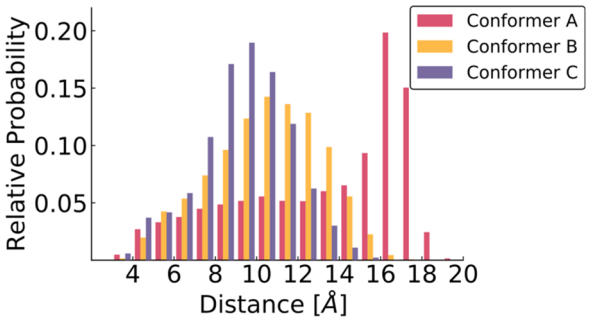

Figure 6. Distribution of distances between the extremes of the palmitate molecule for each of the conformers (A, B, and C) of *holo*-Na-FAR-1 during the MD simulation.

ligand, while the bent conformation is mainly present on the other two conformers (B and C). Since the three *holo*-Na-FAR-1 conformers are in dynamics equilibrium during the MD simulation (see Figure 4c), the ligand changes its conformation accordingly to the corresponding changes in the cavity sizes associated with each protein conformational change.

Finally, MD simulations have been performed on the orthologue Ce-FAR-7 in its *apo*-conformation. Figure 7b shows the average structure obtained from the corresponding equilibrated MD simulation. Ce-FAR-7 is an orthologue of Na-FAR-1 that, despite its similar overall fold, it presents an internal cavity different in size and shape respect to Na-FAR-1.[20] Therefore, a comparison of the relative flexibility of the ligand-binding cavities for Ce-FAR-7 and Na-FAR-1 can enlighten on the origin of the differences in their ligand binding and biological properties.

The RMSD between average *apo*-Na-FAR-1 and *apo*-Ce-FAR-7 is 2.77 Å. In agreement with *apo*-Na-FAR-1, Figure 7a shows that the distribution of its internal cavity volume can be associated with protein fluctuations around a unique conformation characterized by a free energy landscape with a relatively deep well. These results are in agreement with the observations made by Rey-Burusco et al.[20] where the estimated cavity for Ce-FAR-7 calculated revealed a much smaller size than for both forms of Na-FAR-1.

3.2. β-Barrel FABPs. While FARs exhibit α-helix rich folds, most FABPs present a typical FABP β-barrel fold that includes a small and displaced hydrophobic core and a cavity filled with water molecules. In order to understand how the different folds impact on the protein properties associated with the transport of a variety of ligands with different shapes and sizes, MD simulations have been performed on the rat intestinal fatty-acid-binding protein (I-FABP) in its *holo* and *apo* forms. The ligand-binding conformational change involves a structural distortion with a RMSD = 1.00 Å. The average internal ligand-cavity is significantly smaller than Na-FAR-1, being 605 ± 145 and 926 ± 85 Å^3 for *apo*-I-FABP and *holo* I-FABP respectively (see Figure 8). We can observe that the distribution of cavity volumes for *apo*-I-FABP can be associated with the contribution of different conformations explored during the MD simulation. On the contrary, ligand-binding funnels *holo*-I-FABP onto a unique rigid state. These results are in good agreement with previous NMR measurements performed on human L-FABP[71] and rat I-FABP[72] that describe ligand binding as a transition of the protein structure from a slightly more disordered and flexible *apo*-state to a more ordered *holo*-state. Additionally, limited proteolysis experiments performed on apo- and holo- rat IFABP showed that the holo-form was resistant to overnight treatment while apo-IFABP was fully degraded.[73,74] This analysis have also been applied on cestodes FABPs yielding the same result.[75] Besides, the comparison of RMSF obtained during our MD simulations indicates larger fluctuations for the *apo*- than for the *holo*- I-FABP (see Figure S1). This is in good agreement with the results of Matsuoka et al.[40] where the authors show that the calculated RMSF values were less than 1.0 Å for almost all protein residues, indicating that this protein is rigid in the ligand-bound form. This increased mobility and discrete disorder in the *apo*-state may facilitate the entry of the ligand into the cavity.

PCA allows the identification of the different *apo*-I-FABP conformers and their corresponding effect on the volume of the internal cavity (see Figure 9a,b). Four different conformers, associated with different combinations of structural distortions in the directions of the first and second PCA modes, have been identified (see also Figure S3 and Figure S4). Two of them (A and B) are associated with smaller cavity volumes than the other two(C and D). Figures 9c shows that *apo*-I-FABP experiences multiple conformational changes throughout the MD simulation, indicating a relatively low energy barrier between its states. On the contrary, the projection of the set of MD snapshots of *holo*-I-FABP onto its first and second PCA modes does not reveal the existence of multiple conformers but rather a unique rigid state (see Figure S5). This is in agreement with the distribution of its cavity volumes, shown in Figure 8c, represented as a Gaussian distribution that can be associated with fluctuations around a unique minimum in the protein conformational space. Ligand binding seems to shift the conformational equilibrium of I-FABP to a unique conformation with a sufficiently deep well to ensure that a significant fraction of protein molecules are trapped fluctuating in it.

3.3. Relative Flexibility of the Ligand-Cavities. The different FARs and FABPs analyzed in this study have shown

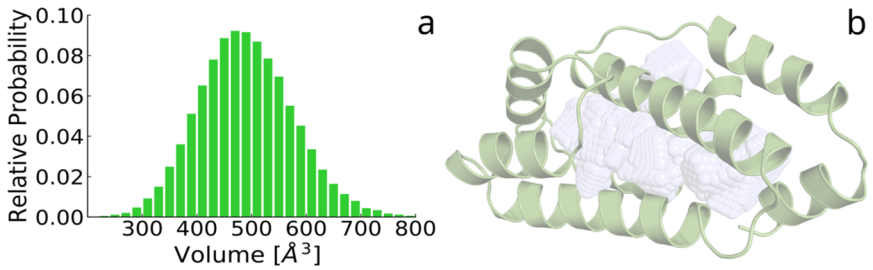

Figure 7. (a) Distribution of its internal cavity volume, calculated over the set of collected MD structures. (b) Averaged structure of *apo*-Ce-FAR-7 obtained from the equilibrated MD simulation.

DOI: 10.1021/acs.jcim.9b00364
J. Chem. Inf. Model. XXXX, XXX, XXX−XXX

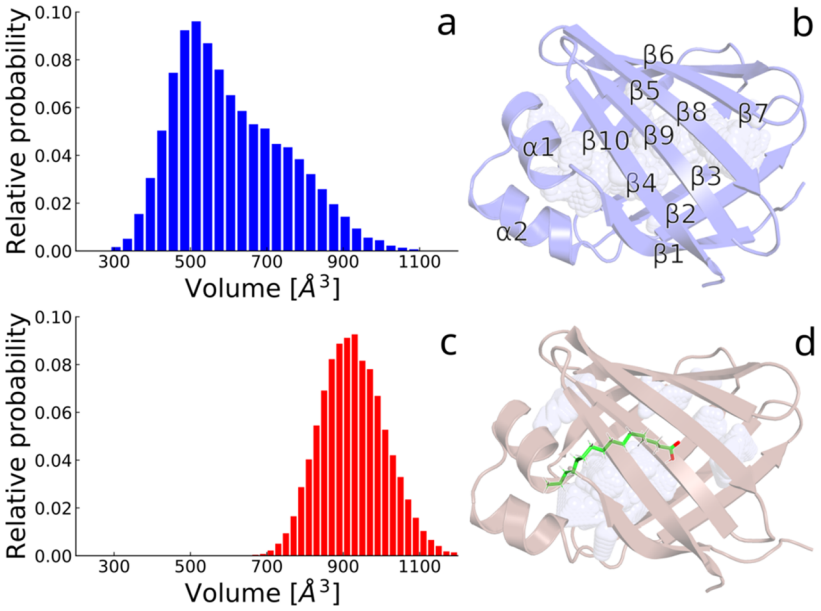

Figure 8. Distribution of ligand cavity volumes, calculated over the set of structures collected during the equilibrated MD simulations of (a) *apo*- and (c) *holo*- I-FABP. Averaged (b) *apo*- and (d) *holo*-structures for I-FABP obtained from the corresponding equilibrated MD simulations, indicating the main secondary structure elements (SSE) and the encompass ligand cavity.

ligand-cavities with different shapes whose dynamics is subject to the corresponding protein plasticity. In order to analyze which LBP fold encompasses a more flexible cavity and, therefore, a cavity that can contribute to a larger ligand multiplicity, we calculated the variation of the potential energy of each LBP in the direction of $\nabla \mathbf{V}_o$ (see section 2.3). Results are shown in Figure 10a. We consider the amplitude of the displacement in the direction of $\nabla \mathbf{V}_o$ achieved with an energy equal to kT = 0.593 kcal/mol (with k being the Boltzman's constant and T = 298 K) as a measure of flexibility of the cavity.[53] We can observe that the internal cavity of *apo*-I-FABP results the most flexible one, followed by *holo*- and *apo*-Na-FAR-1. *Apo*-Ce-FAR-7 presents a relatively more rigid cavity. Besides, the two *holo*-I-FABPs (1URE and 2IFB) enclose the most rigid cavities, reinforcing the idea that β-barrel I-FABPs follow a ligand-binding strategy involving a *holo*-state with restricted motional freedom.

While both *holo*-Na-FAR-1 and *apo*-I-FABP encompass cavities with different sizes according to the transient protein conformation, Figure 10b,c displays the analysis of the corresponding individual conformers. We can observe that, in both cases, each conformer result relatively more rigid than the average shown in Figure 10a, indicating that their individual contributions introduce an additional component to the overall flexibility of the cavity. Furthermore, *holo*-Na-FAR-1 conformers are less rigid than the average (see Figure 10b) compared to *apo*-I-FABP conformers relative to their corresponding average (see Figure 10c). That is, the flexibility of *holo*-Na-FAR-1 seems to be more uniformly distributed among the conformer populations in dynamic equilibrium. Therefore, we conclude that the native state of I-FABP, defined as an equilibrium of pre-existing populations of states, can be considered in general more flexible than the native state of I-FABP. These results indicate a propensity of Na-FAR-1 to bind not only fatty acids but also a broader range of lipid classes such as retinol and phospholipids. This feature is in agreement with previous fluorescence experiments performed on Na-FAR-1 and Ce-FAR-7.[20]

4. CONCLUSIONS

Parasitic helminths produce and release an unexpectedly wide range of LBPs that are structurally distinct from those of their hosts. Although poorly understood, helminth LBPs are often immunodominant in infection. Some of them attract allergic-type antibody responses and have been associated with protective immunity.[4,76−78] The evolutionary reasons why a single species expresses different types of LBPs remain unclear. FARs are commonly found in the secretions of parasitic nematodes, possibly indicating their role in parasitism. Parasites need to acquire nutrients from their hosts and they also need to defend themselves against immune response from the host. In this sense, it is hypothesized that they interfere by sequestering signaling lipids produced by the host. Therefore, a large ligand multiplicity of FARs would help in both lipid acquisition and sequestering. As mentioned before they have also been proven as good vaccine candidates.[13]

Protein fluctuations−cavity changes relationships have been explored on different α-helix rich FARs and β-barrel FABPs using long equilibrated MD simulations of either *apo*- and *holo*-states. We found a significantly flexible Na-FAR-1 ligand-cavity that can explain the observed larger ligand multiplicity of α-helix FARs respect to β-barrel FABPs. The comparison of the relative flexibility of ligand-binding cavities of Ce-FAR-7 and Na-FAR-1 reveals how a similar fold can enclose internal cavities with significant differences in their flexibilities and dynamics. These differences can explain differences in their ligand multiplicity and, therefore, their biological function. Moreover, differences in ligand binding capacities have been observed between two isoforms from the same species.[13]

We have reported two different ligand-binding strategies. Particularly, *holo*-Na-FAR-1 presents a remarkable conformational plasticity that drives a complex internal cavity dynamics involving different states. The size of the cavity is significantly affected by protein conformational changes. Besides, the ligand also changes its conformation according to these conformational changes. That is, far from being fixed within the cavity,

DOI: 10.1021/acs.jcim.9b00364
J. Chem. Inf. Model. XXXX, XXX, XXX−XXX

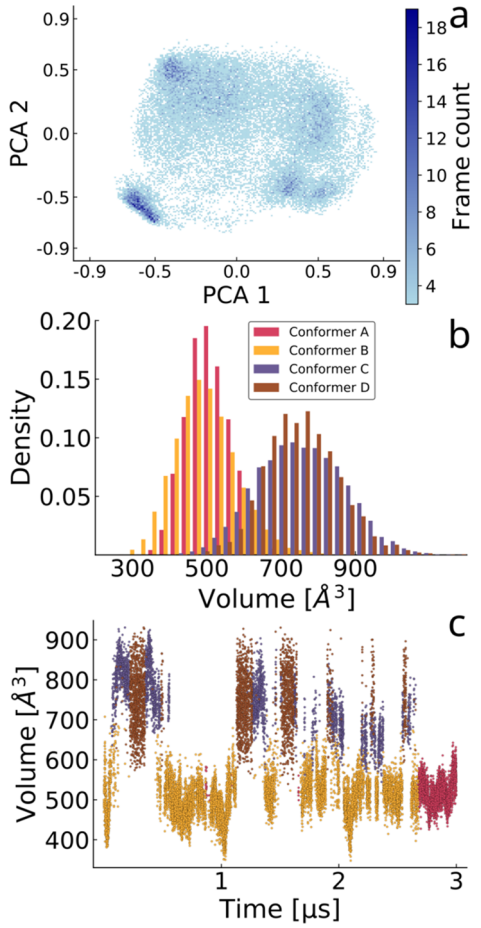

Figure 9. (a) Contour density plots of the projection of the set of MD snapshots of *apo*-I-FABP onto its 1st and 2nd PCA modes; (b) distribution of cavity volumes for each of the *apo*-I-FABP conformers (A, B, C, and D) during the MD simulation; (c) evolution in time of the cavity volume displaying the different contributions of each of the four conformers A, B, C, and D conformers.

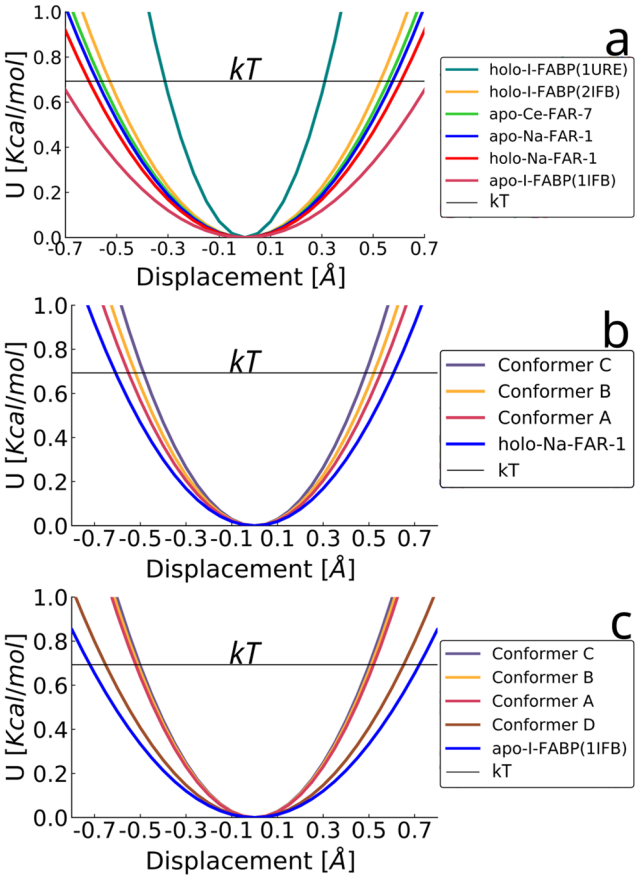

Figure 10. Potential energy change in the direction of ∇V_{ol} for each (a) protein structure, (b) *holo*-Na-FAR-1 conformer, and (c) *apo*-I-FABP conformer. The black line indicated as kT= 0.593 kcal/mol (with k being the Boltzman's constant and T = 298 K) has been added as reference of the average energy per degree of freedom at room temperature.

the ligand experiences large conformational changes between a bent and stretch conformation. The ligand conformation changes according to the size of the cavity that is dictated by the transient protein conformation. On the contrary, ligand binding in I-FABPs seems to shift the conformational equilibrium to a unique conformation. In this way, α-helix FARs and β-barrel FABPs seem to follow two different strategies for ligand-binding. FARs involve a *holo*-state with high plasticity; they experience conformational changes that significantly impact on the cavity volume and embedded ligand conformations. On the other hand, FABPs experience an inverse ligand-modulated disorder−order transition leading to a *holo*-state with restricted motional freedom. This piece of information could give light on the biological reasons for the existence of different LBPs types in the same organism.

Human hookworm infections represent a significant problem in South America. There is an urgent need to design new treatments based on the knowledge of the metabolism of the parasites. Na-FAR1 has shown to be part of the excretion/secretion products, playing an important role in the host-parasite relationship. It may participate in the acquisition of lipids from the host or sequestering signaling molecules dampening the immune response from the host. The detailed knowledge of the structural and dynamics properties of its ligand-binding cavity could contribute to the design of new and more specific inhibitors. The flexibility of protein cavities impacts on functional aspects like ligand affinities and binding promiscuities. The present work can encourage the development of drugs that rigidize the cavity of Na-FAR-1, reducing its ligand multiplicity and, therefore, the efficiency to play its biological function.

■ ASSOCIATED CONTENT

Supporting Information

The Supporting Information is available free of charge on the ACS Publications website at DOI: 10.1021/acs.jcim.9b00364.

Table S1: List of residues lining the main ligand-binding cavity for each system. Residues are numbered according to their order in the corresponded PDB file. Figure S1: Root mean square fluctuations (RMSF) during our MD simulations. Figure S2: Histogram of the projection of the set of MD snapshots of holo-I-FABP onto its third PCA mode. Figure S3: First (red) and second (blue) PCA modes of (a) apo- and (b) holo-I-FABP. Figure S4: Superposition of the four conformers (A, B, C, and D) of apo-I-FABP. Figure S5: Contour density plots of the projection of the set of MD snapshots of holo-I-FABP onto their corresponding first and second PCA modes (PDF)

DOI: 10.1021/acs.jcim.9b00364
J. Chem. Inf. Model. XXXX, XXX, XXX−XXX

AUTHOR INFORMATION

Corresponding Author

*E-mail: sfalberti@gmail.com.

ORCID

G. P. Barletta: 0000-0002-0806-0812

S. Fernandez-Alberti: 0000-0002-0916-5069

Notes

The authors declare no competing financial interest.

REFERENCES

(1) Lucke, C.; Gutierrez-Gonzales, L. H.; Hamilton, J. Intracellular Lipid Binding Proteins: Evolution, Structure, and Ligand Binding. In *Cellular proteins and their ligand fatty acids—emerging roles in gene expression, health and disease*; Duttaroy, A., Spener, F., Eds.; Wiley: New York, 2003; pp 95−114.

(2) Franchini, G.; Pórfido, J.; Ibáñez Shimabukuro, M.; Rey Burusco, M.; Bélgamo, J.; Smith, B.; Kennedy, M.; Córsico, B. The Unusual Lipid-Binding Proteins of Parasitic Helminths and Their Potential Roles in Parasitism and as Therapeutic Targets. *Prostaglandins, Leukotrienes Essent. Fatty Acids* **2015**, *93*, 31−36.

(3) Barrett, J. Forty Years of Helminth Biochemistry. *Parasitology* **2009**, *136* (12), 1633−1642.

(4) Mei, B.; Kennedy, M. W.; Beauchamp, J.; Komuniecki, P. R.; Komuniecki, R. Secretion of a Novel, Developmentally Regulated Fatty Acid-Binding Protein into the Perivitelline Fluid of the Parasitic Nematode, Ascaris Suum. *J. Biol. Chem.* **1997**, *272*, 9933−9941.

(5) Plenefisch, J.; Xiao, H.; Mei, B. S.; Geng, J. M.; Komuniecki, P. R.; Komuniecki, R. Secretion of a Novel Class of IFABPs in Nematodes: Coordinate Use of the Ascaris/Caenorhabditis Model Systems. *Mol. Biochem. Parasitol.* **2000**, *105*, 223−236.

(6) Garofalo, A.; Rowlinson, M. C.; Amambua, N. A.; Hughes, J. M.; Kelly, S. M.; Price, N. C.; Cooper, A.; Watson, D. G.; Kennedy, M. W.; Bradley, J. E. The FAR Protein Family of the Nematode Caenorhabditis Elegans - Differential Lipid Binding Properties, Structural Characteristics, and Developmental Regulation. *J. Biol. Chem.* **2003**, *278*, 8065−8074.

(7) Jones, J. T.; Kumar, A.; Pylypenko, L. A.; Thirugnanasambandam, A.; Castelli, L.; Chapman, S.; Cock, P. J.; Grenier, E.; Lilley, C. J.; Phillips, M. S.; Blok, V. C. Identification and Functional Characterization of Effectors in Expressed Sequence Tags from Various Life Cycle Stages of the Potato Cyst Nematode Globodera Pallida. *Mol. Plant Pathol.* **2009**, *10*, 815−828.

(8) Kennedy, M. W.; Garside, L. H.; Goodrick, L. E.; McDermott, L.; Brass, A.; Price, N. C.; Kelly, S. M.; Cooper, A.; Bradley, J. E. The Ov20 Protein of the Parasitic Nematode Onchocerca Volvulus - a Structurally Novel Class of Small Helix-Rich Retinol-Binding Proteins. *J. Biol. Chem.* **1997**, *272*, 29442−29448.

(9) Iberkleid, I.; Vieira, P.; de Almeida Engler, J.; Firester, K.; Spiegel, Y.; Horowitz, S. B. Fatty Acid-and Retinol-Binding Protein, Mj-FAR-1 Induces Tomato Host Susceptibility to Root-Knot Nematodes. *PLoS One* **2013**, *8*, e64586.

(10) Solovyova, A.; Meenan, N.; McDermott, L.; Garofalo, A.; Bradley, J.; Kennedy, M.; Byron, O. The Polyprotein and FAR Lipid Binding Proteins of Nematodes: Shape and Monomer/Dimer States in Ligand-Free and Bound Forms. *Eur. Biophys. J.* **2003**, *32* (5), 465−476.

(11) Fairfax, K. C.; Vermeire, J. J.; Harrison, L. M.; Bungiro, R. D.; Grant, W.; Husain, S. Z.; Cappello, M. Characterisation of a Fatty Acid and Retinol Binding Protein Orthologue from the Hookworm Ancylostoma Ceylanicum. *Int. J. Parasitol.* **2009**, *39*, 1561−1571.

(12) Burbelo, P. D.; Leahy, H. P.; Iadarola, M. J.; Nutman, T. B. A Four-Antigen Mixture for Rapid Assessment of Onchocerca Volvulus Infection. *PLoS Neglected Trop. Dis.* **2009**, *3*, e438.

(13) Zhan, B.; Arumugam, S.; Kennedy, M.; Tricoche, N.; Lian, L.-Y.; Asojo, O.; Bennuru, S.; Bottazzi, M.; Hotez, P. J.; Lustigman, S.; Klei, T. R. Ligand Binding Properties of Two Brugia Malayi Fatty Acid and Retinol (FAR) Binding Proteins and Their Vaccine Efficacies against Challenge Infection in Gerbils. *PLoS Neglected Trop. Dis.* **2018**, *12* (10), e0006772.

(14) Lal, P. G.; James, E. R. Onchocerca Retinol- and Ivermectin-Binding Protein Activity. *Parasitology* **1996**, *112* (2), 221−225.

(15) Sani, B.; Vaid, A. Specific Interaction of Ivermectin with Retinol-Binding Protein from Filarial Parasites. *Biochem. J.* **1988**, *249*, 929−932.

(16) Vos, T.; et al. Global, Regional, and National Incidence, Prevalence, and Years Lived with Disability for 328 Diseases and Injuries for 195 Countries, 1990−2016: A Systematic Analysis for the Global Burden of Disease Study. *Lancet* **2017**, *390* (10100), 1211−1259.

(17) Loukas, A.; Hotez, P.; Diemert, D.; Yazdanbakhsh, M.; McCarthy, J.; Correa-Oliveira, R.; Croese, J.; Bethony, J. Hookworm Infection. *Nat. Rev. Dis Prim.* **2016**, *2* (1), 16088.

(18) Zonta, M.; Oyhenart, E.; Navone, G. Nutritional Status, Body Composition, and Intestinal Parasitism among the Mbyá-Guaraní Communities of Misiones, Argentina. *Am. J. Hum Biol.* **2009**, *22* (2), 193−200.

(19) Daub, J.; Loukas, A.; Pritchard, D.; Blaxter, M. A Survey of Genes Expressed in Adults of the Human Hookworm, Necator Americanus. *Parasitology* **2000**, *120* (2), 171−184.

(20) Rey-Burusco, M.; Ibañez-Shimabukuro, M.; Gabrielsen, M.; Franchini, G.; Roe, A.; Griffiths, K.; Zhan, B.; Cooper, A.; Kennedy, M. W.; Córsico, B.; Smith, B. O. Diversity in the Structures and Ligand-Binding Sites of Nematode Fatty Acid and Retinol-Binding Proteins Revealed by Na-FAR-1 from Necator Americanus. *Biochem. J.* **2015**, *471*, 403−414.

(21) Jordanova, R.; Groves, M.; Kostova, E.; Woltersdorf, C.; Liebau, E.; Tucker, P. Fatty Acid- and Retinoid-Binding Proteins Have Distinct Binding Pockets for the Two Types of Cargo. *J. Biol. Chem.* **2009**, *284* (51), 35818−35826.

(22) Storch, J.; McDermott, L. Structural and Functional Analysis of Fatty Acid-Binding Proteins. *J. Lipid Res.* **2009**, *50* (Suppl), S126−S131.

(23) Storch, J.; Corsico, B. The Emerging Functions and Mechanisms of Mammalian Fatty Acid-Binding Proteins. *Annu. Rev. Nutr.* **2008**, *28*, 73−95.

(24) Banaszak, L.; Winter, N.; Xu, Z.; Bernlohr, D.; Cowan, S.; Jones, T. Lipid-Binding Proteins: A Family of Fatty Acid and Retinoid Transport Proteins. *Adv. Protein Chem.* **1994**, *45*, 89−151.

(25) Stewart, J. The Cytoplasmic Fatty-Acid-Binding Proteins: Thirty Years and Counting. *Cell. Mol. Life Sci.* **2000**, *57*, 1345−1359.

(26) Friedman, R.; Nachliel, E.; Gutman, M. Fatty Acid Binding Proteins : Same Structure but Different Binding Mechanisms ? Molecular Dynamics Simulations of Intestinal Fatty Acid Binding Protein. *Biophys. J.* **2006**, *90* (March), 1535−1545.

(27) Hotamisligil, G.; Bernlohr, D. Metabolic Functions of FABPs-Mechanisms and Therapeutic Implications. *Nat. Rev. Endocrinol.* **2015**, *11* (10), 592−605.

(28) McDermott, L.; Cooper, A.; Kennedy, M. Novel Classes of Fatty Acid and Retinol Binding Protein from Nematodes. *Mol. Cell. Biochem.* **1999**, *192*, 69−75.

(29) Zimmerman, A. W.; Veerkamp, J. H. New Insights into the Structure and Function of Fatty Acid-Binding Proteins. *Cell. Mol. Life Sci.* **2002**, *59*, 1096−1116.

(30) Veerkamp, J.; Peeters, R.; RGHJ, M. Structural and Functional Features of Different Types of Cytoplasmic Fatty Acid-Binding. *Biochim. Biophys. Acta, Lipids Lipid Metab.* **1991**, *1081*, 1−24.

(31) Sha, R.; Kane, C.; Xu, Z.; Banaszak, L.; Bernlohr, D. Modulation of Ligand Binding Affinity of the Adipocyte Lipid-Binding Protein by Selective Mutation: Analysis in Vitro and in Situ. *J. Biol. Chem.* **1993**, *268*, 7885−7892.

(32) Prinsen, C.; Veerkamp, J. Fatty Acid Binding and Conformational Stability of Mutants of Human Muscle Fatty Acid-Binding Protein. *Biochem. J.* **1996**, *314*, 253−260.

(33) Jakoby, M.; Miller, K.; Toner, J.; Bauman, A.; Cheng, L.; Li, E.; et al. Ligand-Protein Electrostatic Interactions Govern the Specificity

DOI: 10.1021/acs.jcim.9b00364
J. Chem. Inf. Model. XXXX, XXX, XXX−XXX

of Retinol- and Fatty Acid-Binding Proteins. *Biochemistry* **1993**, *32*, 872−878.
(34) Thumser, A.; Evans, C.; Worrall, A.; Wilton, D. Effect on Ligand Binding of Arginine Mutations in Recombinant Rat Liver Fatty Acid-Binding Protein. *Biochem. J.* **1994**, *297*, 103−107.
(35) Thumser, A.; Voysey, J.; Wilton, D. Mutations of Recombinant Rat Liver Fatty Acid-Binding Protein at Residues 102 and 122 Alter Its Structural Integrity and Affinity for Physiological Ligands. *Biochem. J.* **1996**, *314*, 943−949.
(36) Laulumaa, S.; Nieminen, T.; Raasakka, A.; Krokengen, O.; Safaryan, A.; Hallin, E.; Brysbaert, G.; Lensink, M.; Ruskamo, S.; Vattulainen, I.; Kursula, P. Structure and Dynamics of a Human Myelin Protein P2 Portal Region Mutant Indicate Opening of the β Barrel in Fatty Acid Binding Proteins. *BMC Struct. Biol.* **2018**, *18* (8), 1−13.
(37) Hodsdon, M. E.; Cistola, D. P. Discrete Backbone Disorder in the Nuclear Magnetic Resonance Structure of Apo Intestinal Fatty Acid-Binding Protein: Implications for the Mechanism of Ligand Entry. *Biochemistry* **1997**, *36*, 1450−1460.
(38) Friedman, R.; Nachliel, E.; Gutman, M. Molecular Dynamics Simulations of the Adipocyte Lipid Binding Protein Reveal a Novel Entry Site for the Ligand. *Biochemistry* **2005**, *44*, 4275−4283.
(39) Tsfadia, Y.; Friedman, R.; Kadmon, J.; Selzer, A.; Nachliel, E.; Gutman, M. Molecular Dynamics Simulations of Palmitate Entry into the Hydrophobic Pocket of the Fatty Acid Binding Protein. *FEBS Lett.* **2007**, *581* (6), 1243−1247.
(40) Matsuoka, D.; Sugiyama, S.; Murata, M.; Matsuoka, S. Molecular Dynamics Simulations of Heart-Type Fatty Acid Binding Protein in Apo and Holo Forms, and Hydration Structure Analyses in the Binding Cavity. *J. Phys. Chem. B* **2015**, *119* (1), 114−127.
(41) Laulumaa, S.; Nieminen, T.; Lehtimäki, M.; Aggarwal, S.; Simons, M.; Koza, M. M.; Vattulainen, I.; Kursula, P.; Natali, F. Dynamics of the Peripheral Membrane Protein P2 from Human Myelin Measured by Neutron Scattering—A Comparison between Wild-Type Protein and a Hinge Mutant. *PLoS One* **2015**, *10* (6), e0128954.
(42) Guo, Y.; Duan, M.; Yang, M. The Observation of Ligand-Binding-Relevant Open States of Fatty Acid Binding Protein by Molecular Dynamics Simulations and a Markov State Model. *Int. J. Mol. Sci.* **2019**, *20* (14), 3476.
(43) Andrew McCammon, J.; Harvey, S. C. *Dynamics of Proteins and Nucleic Acids*; Cambridge University Press: Cambridge, U.K., 1987.
(44) Karplus, M.; Kuriyan, J. Molecular Dynamics and Protein Function. *Proc. Natl. Acad. Sci. U. S. A.* **2005**, *102*, 6679−6685.
(45) Karplus, M.; McCammon, J. A. Molecular Dynamics Simulations of Biomolecules. *Nat. Struct. Biol.* **2002**, *9*, 646−652.
(46) Brooks, C., III; Karplus, M.; Pettitt, B. M. *Proteins: A Theoretical Perspective of Dynamics, Structure, and Thermodynamics*; Prigogine, I., Rice, S. A., Eds.; John Wiley & Sons Ltd.: New York, 1987.
(47) Ichiye, T.; Karplus, M. Collective Motions in Proteins: A Covariance Analysis of Atomic Fluctuations in Molecular Dynamics and Normal Mode Simulations. *Proteins: Struct., Funct., Genet.* **1991**, *11*, 205−217.
(48) Horiuchi, T.; Go, N. Projection of Monte Carlo and Molecular Dynamics Trajectories onto the Normal Mode Axes: Human Lysozyme. *Proteins: Struct., Funct., Genet.* **1991**, *10* (2), 106−116.
(49) van Aalten, D. M. F.; de Groot, B. L.; Findlay, J. B. C.; Berendsen, H. J. C.; Amadei, A. A Comparison of Techniques for Calculating Protein Essential Dynamics. *J. Comput. Chem.* **1997**, *18* (2), 169−181.
(50) Jolliffe, I. T. *Principal Component Analysis*, 2nd ed.; Springer-Verlag: Berlin, 2002.
(51) David, C. C.; Jacobs, D. J. *Protein Dynamics*; Livesay, D. R., Ed.; Methods in Molecular Biology; Humana Press: Totowa, NJ, 2014; Vol. *1084*.
(52) Desdouits, N.; Nilges, M.; Blondel, A. Principal Component Analysis Reveals Correlation of Cavities Evolution and Functional Motions in Proteins. *J. Mol. Graphics Modell.* **2015**, *55*, 13−24.
(53) Barletta, G. P.; Fernandez-Alberti, S. Protein Fluctuations and Cavity Changes Relationship. *J. Chem. Theory Comput.* **2018**, *14* (2), 998−1008.
(54) *Lipid Binding Proteins within Molecular and Cellular Biochemistry*; Banaszak, L., Bernlohr, D. A., Eds.; Springer Science +Business Media, B.V.: Berlin.
(55) Hunter, N. H.; Bakula, B. C.; Bruce, C. D. Molecular Dynamics Simulations of Apo and Holo Forms of Fatty Acid Binding Protein 5 and Cellular Retinoic Acid Binding Protein II Reveal Highly Mobile Protein, Retinoic Acid Ligand, and Water Molecules. *J. Biomol. Struct. Dyn.* **2018**, *36* (7), 1893−1907.
(56) Rich, M.; Evans, J. S. Molecular Dynamics Simulations of Adipocyte Lipid-Binding Protein: Effect of Electrostatics and Acyl Chain Unsaturation. *Biochemistry* **1996**, *35* (5), 1506−1515.
(57) Long, D.; Mu, Y.; Yang, D. Molecular Dynamics Simulation of Ligand Dissociation from Liver Fatty Acid Binding Protein. *PLoS One* **2009**, *4* (6), e6081.
(58) Sivanesan, D.; Rajnarayanan, R.; Doherty, J.; Pattabiraman, N. In-Silico Screening Using Flexible Ligand Binding Pockets: A Molecular Dynamics-Based Approach. *J. Comput.-Aided Mol. Des.* **2005**, *19* (4), 213−228.
(59) Salomon-Ferrer, R.; Case, D.; Walker, R. An Overview of the Amber Biomolecular Simulation Package. *WIREs Comput. Mol. Sci.* **2013**, *3*, 198−210.
(60) Case, D.; Cheatham, T. I.; Darden, T.; Gohlke, H.; Luo, R.; Merz, K. J.; Onufriev, A.; Simmerling, C.; Wang, B.; Woods, R. The Amber Biomolecular Simulation Programs. *J. Comput. Chem.* **2005**, *26*, 1668−1688.
(61) Berman, H.; Westbrook, J.; Feng, Z.; Gilliland, G.; Bhat, T. The Protein Data Bank. *Nucleic Acids Res.* **2000**, *28*, 235−242.
(62) Sacchettini, J.; Gordon, J.; Banaszak, L. Refined Apoprotein Structure of Rat Intestinal Fatty Acid Binding Protein Produced in Escherichia Coli. *Proc. Natl. Acad. Sci. U. S. A.* **1989**, *86* (20), 7736−7740.
(63) Sacchettini, J.; Gordon, J.; Banaszakl, L. Crystal Structure of Rat Intestinal Protein Refinement and Analysis of the Escherichia Coli- Derived Protein with Bound Palmitate. *J. Mol. Biol.* **1989**, *208*, 327−339.
(64) Hodsdon, M.; Ponder, J.; Cistola, D. The NMR Solution Structure of Intestinal Fatty Acid-Binding Protein Complexed with Palmitate: Application of a Novel Distance Geometry Algorithm. *J. Mol. Biol.* **1996**, *264*, 585−602.
(65) Ponder, J.; Case, D. Force Fields for Protein Simulations. *Adv. Protein Chem.* **2003**, *66*, 27−85.
(66) Maier, J.; Martinez, C.; Kasavajhala, K.; Wickstrom, L.; Hauser, K.; Simmerling, C. Ff14SB: Improving the Accuracy of Protein Side Chain and Backbone Parameters from Ff99SB. *J. Chem. Theory Comput.* **2015**, *11*, 3696−3713.
(67) Jorgensen, W.; Chandrasekhar, J.; Madura, J.; Impey, R.; Klein, M. Comparison of Simple Potential Functions for Simulating Liquid Water. *J. Chem. Phys.* **1983**, *79*, 926−935.
(68) Amadei, A.; Linssen, A. B. M.; Berendsen, H. J. C. Essential Dynamics of Proteins. *Proteins: Struct., Funct., Genet.* **1993**, *17* (4), 412−425.
(69) Brooks, B.; Janezic, D.; Karplus, M. Harmonic Analysis of Large Systems. I. Methodology. *J. Comput. Chem.* **1995**, *16* (12), 1522−1542.
(70) Monzon, A. M.; Zea, D. J.; Fornasari, M. S.; Saldaño, T. E.; Fernandez-Alberti, S.; Tosatto, S. C. E.; Parisi, G. Conformational Diversity Analysis Reveals Three Functional Mechanisms in Proteins. *PLoS Comput. Biol.* **2017**, *13* (2), e1005398.
(71) Chen, Z.; Qiao, Y.; Klimtchuk, E.; Hamilton, J. A.; Cai, J.; Lu, C. Solution Structure and Backbone Dynamics of Human Liver Fatty Acid Binding Protein : Fatty Acid Binding Revisited. *Biophys. J.* **2012**, *102* (11), 2585−2594.
(72) Hodsdon, M. E.; Cistola, D. P. Ligand Binding Alters the Backbone Mobility of Intestinal Fatty Acid-Binding Protein as Monitored by 15 N NMR Relaxation and 1 H Exchange †. *Biochemistry* **1997**, *36* (8), 2278−2290.

DOI: 10.1021/acs.jcim.9b00364
J. Chem. Inf. Model. XXXX, XXX, XXX−XXX

858 (73) Arighi, C.; Rossi, J.; Delfino, J. Temperature-Induced
859 Conformational Switch in Intestinal Fatty Acid Binding Protein
860 (IFABP) Revealing an Alternative Mode for Ligand Binding.
861 *Biochemistry* **2003**, *42* (24), 7539−7551.
862 (74) Curto, L.; Caramelo, J.; Delfino, J. Delta98delta, a Functional
863 All-Beta-Sheet Abridged Form of Intestinal Fatty Acid Binding
864 Protein.Delta98delta, a Functional All-Beta-Sheet Abridged Form of
865 Intestinal Fatty A. *Biochemistry* **2005**, *44* (42), 13847−13857.
866 (75) Porfido, J.; Alvite, G.; Silva, V.; Kennedy, M.; Esteves, A.;
867 Corsico, B. Direct Interaction between EgFABP1, a Fatty Acid
868 Binding Protein from Echinococcus Granulosus, and Phospholipid
869 Membranes. *PLoS Neglected Trop. Dis.* **2012**, *6* (11), e1893.
870 (76) Garofalo, A.; Kennedy, M.; Bradley, J. The FAR Proteins of
871 Parasitic Nematodes: Their Possible Involvement in the Pathogenesis
872 of Infection and the Use of Caenorhabditis Elegans as a Model
873 System to Evaluate Their Function. *Med. Microbiol. Immunol.* **2003**,
874 *192*, 47−52.
875 (77) Kennedy, M. The Nematode Polyprotein Allergens/Antigens.
876 *Parasitol. Today* **2000**, *16*, 373−380.
877 (78) Kennedy, M.; Scott, J.; Lo, S.; Beauchamp, J.; McManus, D. Sj-
878 FABPcfatty- Acid-Binding Protein of the Human Blood Fluke
879 Schistosoma Japonicum: Structural and Functional Characterization
880 and Unusual Solvent Exposure of a Portal-Proximal Tryptophan
881 Residue. *Biochem. J.* **2000**, *349*, 377−384.

DOI: 10.1021/acs.jcim.9b00364
J. Chem. Inf. Model. XXXX, XXX, XXX−XXX